# SPATIAL COHERENCE AND YOUNG - MICHELSON INTERFEROMETRY

# Jorge García-Sucerquia

Physics department Universidad de Antioquia A. A. 1226, Medellín Fax: (00574) 2638282 jigarcia@pegasus.udea.edu.c

#### (

## Román Castañeda

Physics department Universidad Nacional de Colombia Sede Medellín A. A. 3840, Medellín Fax: (00574) 2604489

rcastane@perseus.unalmed.e du.co

### Francisco F. Medina

Physics department Universidad de Antioquia A. A. 1226, Medellín Fax: (00574) 2638282 fmedina@catios.udea.edu.co

#### Abstract

The intensity distribution at the exit of a Young-Michelson interferometer is analysed on the Fourier domain. The analysis shows that two numbers are necessary for describing properly the variation of the visibility of the interferogram fringes. One of them is the complex degree of spatial coherence, which describes the correlation between the contributions from the Young's slits. The second number, which is independent from the first but also has a spatial meaning, describes the correlation between the Young's interferograms reflected by the mirrors of the compensated Michelson interferometer.

# 1. INTRODUCTION

It has long been recognised that the term *coherence* plays a fundamental role in optics, where it is used to denote the correlation properties to different orders of the optical field. It is generally accepted that complete coherence requires significant correlation values to all orders [1,2].

Observation of higher-order coherence properties, which are described by correlations of higher order, usually requires refined experimental systems. For example, in 1955 Hanbury Brown and Twiss performed a photon correlation experiment described by a quartic correlation [1,2]. In their experiment the correlation was between the photocurrents produced by intensity patterns collected by two different detectors.

Spatial coherence properties revealed by a simple Young's experiment are referred as second order spatial coherence [2], which describes the tendency of two values of the optical field at distantly separated points to take on correlated values [1]. Its basic quantity is the complex degree of spatial coherence [3]. On the other hand, the fringe visibility of a Michelson's interference pattern is related to the temporal coherence properties of the optical field [3]. In a compensated Michelson interferometer the optical path length difference between the arms is smaller than the coherence length of the optical field, so that high contrast fringes are generated at the exit of the interferometer.

We show in this paper that if an adequate Young slit pair is attached at the entrance of a compensated Michelson interferometer, a reduction in the visibility of the Michelson's pattern can be observed. Furthermore, this visibility is different from that of the Young's

pattern. As a consequence, two numbers are necessary for describing properly the visibility of the fringe patterns observed at the exit of a Young-Michelson interferometer. One of them is the complex degree of spatial coherence, which describes the correlation between the contributions from the Young's slits. The second number, which is independent from the first one but also has a spatial meaning, describes the correlation between the Young's interferograms reflected by the mirrors of the compensated Michelson interferometer, that is, the correlation between optical fields that contain a further correlation term. In this sense, this device can provide more precise information about the structure of the spatial coherence of the optical field that illumines the whole system.

#### 2. **BASIC THEORY**

Figure 1 depicts the experimental set-up we have used, a cascade of a Young slit pair and a compensated Michelson interferometer (i.e., the optical path lengths of the two arms differ by less than the coherence length of the optical field). With this system, a far field Young interferogram is reflected at both mirrors of the Michelson interferometer. The reflected interferograms superimpose at a CCD sensor, located at the exit of the device, which records the output intensity distribution. Tilting one of the mirrors of the Michelson interferometer, say M2, introduces relative displacements between the superimposed interferograms, allowing us to observe finer spatial coherence properties of the optical field with which we are concerned.

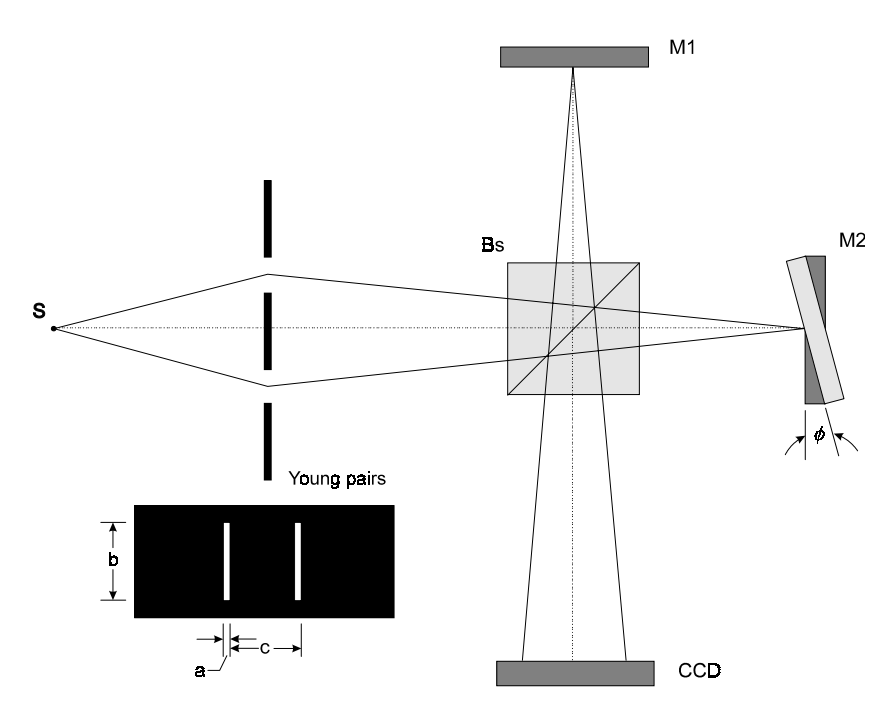


Fig. 1: Experimental set-up of a Young-Michelson interferometer

The intensity distribution recorded by the CCD sensor is determined by the autocorrelation of the amplitude distribution of the optical field there [3]: I(x, y) = W(x, y; x, y), where

$$W(x_1, y_1; x_2, y_2) = \langle V(x_1, y_1) V^*(x_2, y_2) \rangle, \tag{1}$$

where the asterisk denotes complex conjugate and ( ) symbolises the correlation operation. The time-varying complex amplitude  $V(x,y) = A_1(x,y) + A_2(x,y)$ , where  $A_i(x,y)$ , j=1,2, is the amplitude of the contribution at the CCD produced by reflection by the *i*-th mirror of the Michelson interferometer. Thus,

$$W(x_{1}, y_{1}; x_{2}, y_{2}) = \langle A_{1}(x_{1}, y_{1}) + A_{2}(x_{1}, y_{1}), A_{1}^{*}(x_{2}, y_{2}) + A_{2}^{*}(x_{2}, y_{2}) \rangle$$

$$= \langle A_{1}(x_{1}, y_{1}), A_{1}^{*}(x_{2}, y_{2}) \rangle + \langle A_{2}(x_{1}, y_{1}), A_{2}^{*}(x_{2}, y_{2}) \rangle,$$

$$+ 2 \Re e \left[ \langle A_{1}(x_{1}, y_{1}), A_{2}^{*}(x_{2}, y_{2}) \rangle \right]$$
(2)

with  $\Re e$  the real part. The correlation  $\langle A_j(x_1,y_1), A_j^*(x_2,y_2) \rangle$  can be determined by using Zernike's formula in the Fraunhofer domain (far field approach) [3]. Specifically,

$$\langle A_{1}(x_{1}, y_{1}) A_{1}^{*}(x_{2}, y_{2}) \rangle = \left(\frac{1}{\lambda z}\right)^{2} I_{0} \iint \mu_{0}(\xi_{1} - \xi_{2}; \eta_{1} - \eta_{2}) t(\xi_{1}, \eta_{1}) t^{*}(\xi_{2}, \eta_{2})$$

$$\times e^{-i\frac{k}{z}[(x_{1}\xi_{1} + x_{2}\xi_{2}) - (y_{1}\eta_{1} + y_{2}\eta_{2})]} d\xi_{1} d\eta_{1} d\xi_{2} d\eta_{2}$$

$$(3)$$

where  $\lambda$  is the wavelength, z the optical path length for the propagation from the Young slit pair to the CCD sensor,  $I_0$  the intensity across the slits (constant, uniform illumination being assumed), and  $k = \frac{2\pi}{\lambda}$ . The functions  $\mu_0(\xi_1 - \xi_2; \eta_1 - \eta_2)$  and  $t(\xi, \eta)$ represent, respectively, the complex degree of spatial coherence [3] and the transmittance of the Young's slit pair.

Let us assume that the slits are identical and of rectangular shape, with sides a along the  $\xi$  -axis and b>a along the  $\eta$  -axis, so that  $t(\xi,\eta)=1$  inside the slits and zero outside them. Their centres are located on the  $\xi$ -axis and are separated a distance c.

It is possible to prepare the experiment in such a way that

$$\mu_0\left(\xi_1 - \xi_2 \; ; \; \eta_1 - \eta_2\right) = \begin{cases} 1, & \left|\xi_1 - \xi_2\right| \le a \\ \mu = \left|\mu\right| \; \mathcal{C}^{i\,\phi_{12}}, \quad c - a \le \left|\xi_1 - \xi_2\right| \le c + a \end{cases},$$

i.e. the value 1 is taken when the correlated radiators are both inside the same slit and some complex value  $\mu$ , with  $0 \le |\mu| < 1$  and  $\phi_{12}$  constant, when they are located inside different slits. For the sake of simplicity and without lack of generality we assume that  $\phi_{12} = 0$ .

Under the above conditions, Eq. (3) yields

with  $sinc(\pi x) = \frac{sin(\pi x)}{\pi x}$  [4]. A similar formula is obtained for  $\langle A_2(x_1, y_1) A_2^*(x_2, y_2) \rangle$ , but in this case a phase factor should be introduced into the integrand of the Zernike's formula to describe properly the relative displacement of the interferograms at the CCD sensor, with the result

$$\left\langle A_{2}\left(x_{1}, y_{1}\right), A_{2}^{*}\left(x_{2}, y_{2}\right) \right\rangle = 2 \left(\frac{ab}{\lambda z}\right)^{2} I_{0} \operatorname{sinc}\left(\frac{k \ a}{2 \ z} \left(x_{1} - X\right)\right) \operatorname{sinc}\left(\frac{k \ a}{2 \ z} \left(x_{2} - X\right)\right) \operatorname{sinc}\left(\frac{k \ b}{2 \ z} \left(y_{1} - Y\right)\right)$$

$$\times \operatorname{sinc}\left(\frac{k \ b}{2 \ z} \left(y_{2} - Y\right)\right) \left\{ \cos\left[\frac{k \ c}{2 \ z} \left(x_{1} - x_{2}\right)\right] + \left|\mu\right| \cos\left[\frac{k \ c}{2 \ z} \left(x_{1} + x_{2} - 2 \ X\right)\right] \right\}$$

$$(5)$$

where (X,Y) denotes the relative displacement between the interferograms at the CCD sensor plane.

It is useful to introduce the normalised cross-correlation [5]

$$v(x_1, y_1; x_2, y_2) = \frac{\left\langle A_1(x_1, y_1), A_2^*(x_2, y_2) \right\rangle}{\sqrt{I_1^{(\text{max})}} \sqrt{I_2^{(\text{max})}}}, \tag{6}$$

where  $I_j^{(\text{max})}$  is the maximum value of  $I_j(x_j, y_j) = \langle A_j(x_j, y_j), A_j^*(x_j, y_j) \rangle$ , j=1,2, which is the intensity distribution of the Young interferogram reflected by the j-th mirror at the CCD sensor. The intensity distributions  $I_1(x_1, y_1)$  and  $I_2(x_2, y_2)$  can be expressed as

$$I_1(x_1, y_1) = 2 \left(\frac{ab}{\lambda z}\right)^2 I_0 \operatorname{sinc}^2\left(\frac{k \ a}{2 \ z} \ x_1\right) \operatorname{sinc}^2\left(\frac{k \ b}{2 \ z} \ y_1\right) \left\{1 + \ \left|\mu\right| \cos\left(\frac{k \ c}{z} \ x_1\right)\right\}$$
(7a)

and

$$I_{2}(x_{2}, y_{2}) = 2 \left(\frac{ab}{\lambda z}\right)^{2} I_{0} \operatorname{sinc}^{2}\left(\frac{k \ a}{2 \ z} \ (x_{2} - X)\right) \operatorname{sinc}^{2}\left(\frac{k \ b}{2 \ z} \ (y_{2} - Y)\right) \left\{1 + \left|\mu\right| \cos\left(\frac{k \ c}{z} \ (x_{2} - X)\right)\right\}$$
(7b)

The normalised cross-correlation (6) describes the degree of correlation between the contributions reflected by the mirrors of the Michelson interferometer. Indeed, in the far  $v(x_1, y_1; x_2, y_2) = v(x_1, y_1; x_2, y_2) e^{i\left[\frac{k}{2z}\left[(x_1 + x_2)X + (y_1 + y_2)Y\right] + \alpha_{12}\right]}$ whose modulus  $0 \le |v(x_1, y_1; x_2, y_2)| \le 1$  and phase  $\alpha_{12}$  depend on the separation between the points  $(x_1, y_1)$ and  $(x_2, y_2)$ , so that  $\alpha_{ii} = 0$ .

It is reasonable to assume that  $|\nu|$  and  $\alpha_{12}$  are constant for a fixed slit pair and for a specific position of the tilted mirror in our experiment. As before, we assume  $\alpha_{12} = 0$  for the sake of simplicity and without lack of generality. Under this condition and taking into account Eq. (6), the last term of Eq. (2) in the far field approach can be written as

$$2 \Re e \left[ \left\langle A_{1}(x_{1}, y_{1}), A_{2}^{*}(x_{2}, y_{2}) \right\rangle \right] = 2\sqrt{I_{1}(x_{1}, y_{1})} \sqrt{I_{2}(x_{2}, y_{2})} \Re e \left[ v(x_{1}, y_{1}; x_{2}, y_{2}) \right]$$

$$= 2\sqrt{I_{1}(x_{1}, y_{1})} \sqrt{I_{2}(x_{2}, y_{2})} \left| v \left| \cos \left( \frac{k}{2z} \left[ X(x_{1} + x_{2}) + Y(y_{1} + y_{2}) \right] \right) \right|$$
(8)

Furthermore, the intensity distribution recorded by the CCD sensor can be obtained from Eqs. (2), (4), (5) and (8) as

$$I(x,y) = W(x,y; x,y) = 2 \left(\frac{ab}{\lambda z}\right)^{2} I_{0} \left[\operatorname{sinc}^{2}\left(\frac{k}{2} \frac{a}{z} x\right) \operatorname{sinc}^{2}\left(\frac{k}{2} \frac{b}{z} y\right) \left\{1 + |\mu| \cos\left(\frac{k}{z} x\right)\right\} + \operatorname{sinc}^{2}\left(\frac{k}{2} \frac{a}{z} (x-X)\right) \operatorname{sinc}^{2}\left(\frac{k}{2} \frac{b}{z} (y-Y)\right) \left\{1 + |\mu| \cos\left(\frac{k}{z} (x-X)\right)\right\} + 2 \operatorname{sinc}\left(\frac{k}{2} \frac{a}{z} x\right) \operatorname{sinc}\left(\frac{k}{2} \frac{a}{z} (x-X)\right) \operatorname{sinc}\left(\frac{k}{2} \frac{b}{z} (y-Y)\right) + 2 \operatorname{sinc}\left(\frac{k}{2} \frac{a}{z} x\right) \operatorname{sinc}\left(\frac{k}{2} \frac{a}{z} (x-X)\right) \operatorname{sinc}\left(\frac{k}{2} \frac{b}{z} (y-Y)\right) + 2 \operatorname{sinc}\left(\frac{k}{2} \frac{a}{z} x\right) \operatorname{sinc}\left(\frac{k}{2} \frac{a}{z} x\right) \operatorname{sinc}\left(\frac{k}{2} \frac{a}{z} (x-X)\right) + 2 \operatorname{sinc}\left(\frac{k}{2} \frac{a}{z} x\right) \operatorname{sinc}\left(\frac{k}{2} \frac{a}{z} (x-X)\right) + 2 \operatorname{sinc}\left(\frac{k}{2} \frac{a}{z} x\right) \operatorname{sinc}\left(\frac{k}{2} \frac{a}{z} (x-X)\right) + 2 \operatorname{sinc}\left(\frac{k}{2} \frac{a}{z} x\right) \operatorname{sinc}\left(\frac{k}{2} \frac{a}{z} x\right) + 2 \operatorname{sinc}\left(\frac{k}{2} \frac{a}{z} x\right)$$

From Eq. (9) we infer that  $v(x_1, y_1; x_2, y_2)$  is a quantity with spatial meaning but different from the complex degree of spatial coherence  $\mu_0(\xi_1 - \xi_2; \eta_1 - \eta_2)$ . It describes the correlation between the contributions from the Young's slits. So,  $v(x_1, y_1; x_2, y_2)$ describes the spatial correlation of optical fields that contain a correlation term due to a prior Young's interference. Furthermore, these two quantities are necessary to describe properly the intensity distribution of the interferograms.

#### 3. SIMULATIONS, EXPERIMENTAL RESULTS AND DISCUSSION

Figure 2 shows simulated intensity distributions of interferograms described by Eq. (9). They were calculated for different values of |v| with  $|\mu|=1$  and X=Y. The loss of visibility of the Michelson fringes with the decrease of |v| is apparent whereas the high visibility of the Young fringes remains.

Fourier analysis of the interferograms was applied to perform the evaluation of  $|\mu|$  and |v| separately. The Fourier spectrum of the interferogram intensity distributions is given bv

$$\tilde{I}(\xi,\eta) = \int I(x,y) e^{i\frac{k}{z}(x\xi+\eta y)} dx dy$$

$$= \frac{1}{2\pi^{2}} I_{0} \left\{ tri\left(\frac{\xi}{a}, \frac{\eta}{b}\right) \otimes \left\{ \delta(\xi,\eta) + \frac{|\mu|}{2} \left[ \delta(\xi+c,\eta) + \delta(\xi-c,\eta) \right] \right\} \right.$$

$$+ tri\left(\frac{\xi}{a}, \frac{\eta}{b}\right) e^{i\frac{k}{z}(X\xi+Y\eta)} \otimes \left\{ \delta(\xi,\eta) + \frac{|\mu|}{2} e^{i\frac{k}{z}X\xi} \left[ \delta(\xi+c,\eta) + \delta(\xi-c,\eta) \right] \right\}$$

$$+ rect\left(\frac{\xi}{a}, \frac{\eta}{b}\right) \otimes rect\left(\frac{\xi}{a}, \frac{\eta}{b}\right) e^{i\frac{k}{z}(X\xi+Y\eta)} \otimes H(\xi) \delta(\eta) \otimes H(\xi) \delta(\eta) e^{i\frac{k}{z}X\xi}$$

$$\otimes |\nu| \left[ \delta(\xi+X, \eta+Y) + \delta(\xi-X, \eta-Y) \right] \right\} \tag{10}$$

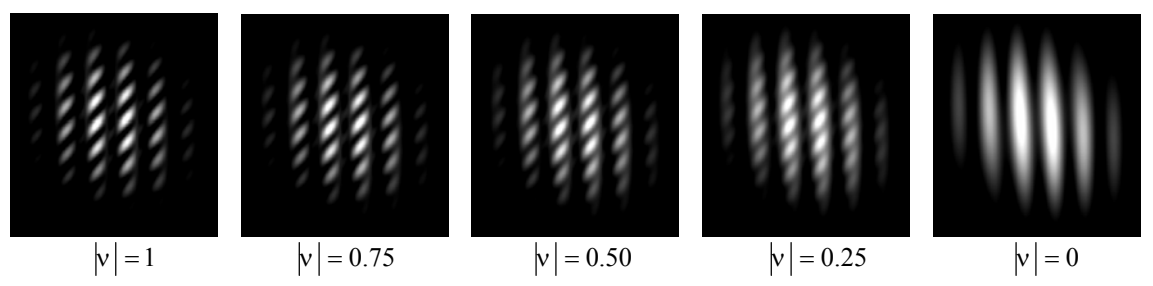


Fig. 2: Simulated intensity distributions of interferograms at the exit of a Young-Michelson interferometer

where  $\otimes$  denotes convolution and the functions that appear in Eq. (10) are defined as follows [4]:

• 
$$\operatorname{tri}\left(\frac{\xi}{a}, \frac{\eta}{b}\right) = \begin{cases} \left(1 - \frac{|\xi|}{a} - \frac{|\eta|}{b} + \frac{|\xi| |\eta|}{a |b|}\right) & (\xi, \eta) \in \mathbf{R} \\ 0 & otherwise \end{cases}$$

with **R** the region limited by the four straight lines  $|\xi| = a$  and  $|\eta| = b$ ,

- $\delta(\xi,\eta)$  is the Dirac's delta function,
- $\operatorname{rect}\left(\frac{\xi}{a}, \frac{\eta}{b}\right) = \begin{cases} 1 & |\xi| \le \frac{a}{2} \text{ and } |\eta| \le \frac{b}{2}, \\ 0 & \text{otherwise} \end{cases}$
- $H(\xi)$  is the Fourier spectrum of  $\sqrt{1+|\mu|\cos\left(\frac{kc}{z}x\right)}$ . It is useful to expand this latter function in a series before the calculation of its Fourier spectrum. Thus, we have [6]

$$\sqrt{1+ |\mu| \cos\left(\frac{k c}{z} x\right)} = \sum_{n=0}^{\infty} \beta_n |\mu|^n \cos^n\left(\frac{k c}{z} x\right)$$

$$= 1 + \sum_{n=1}^{\infty} \left\{ \frac{\beta_{2n}}{2^{2n}} |\mu|^{2n} \left[ \binom{2n}{n} + \sum_{j=0}^{n-1} 2 \binom{2n}{j} \cos\left((n-j) \frac{2 k c}{z} x\right) \right] + \frac{\beta_{2n-1}}{2^{2(n-1)}} |\mu|^{2n-1} \sum_{j=0}^{n-1} \binom{2n-1}{j} \cos\left((n-j-\frac{1}{2}) \frac{2 k c}{z} x\right) \right\}$$

$$(11)$$

where the coefficients  $\beta_n$  are given by  $\beta_0 = 1$ ,  $\beta_1 = \frac{1}{2}$ ,  $\beta_2 = \frac{1}{8}$ ,  $\beta_3 = \frac{3}{48}$ ,  $\beta_4 = -\frac{15}{384}$ , ... The Fourier spectrum of this expression is thus

$$H(\xi) = \delta(\xi) + \sum_{n=1}^{\infty} \left\{ \frac{\beta_{2n}}{2^{2n}} |\mu|^{2n} \left[ \binom{2n}{n} \delta(\xi) + \sum_{j=0}^{n-1} \binom{2n}{j} \left[ \delta(\xi + 2(n-j)c) + \delta(\xi - 2(n-j)c) \right] \right] + \frac{\beta_{2n-1}}{2^{2(n-1)+1}} |\mu|^{2n-1} \sum_{j=0}^{n-1} \binom{2n-1}{j} \left[ \delta(\xi + 2(n-j-1)c) + \delta(\xi - 2(n-j)c) \right] \right\}$$

$$(12)$$

From Eqs. (10) to (12) we conclude that  $\tilde{I}(\xi,\eta)$  will consists of a set of peaks, distributed as follows (Fig.3):

- The first two terms in Eq. (10) correspond to the Young interferograms, without regard for the modulation by Michelson fringes. They consist of three peaks with pyramidal profiles, one of them at the origin of the coordinates  $(\xi,\eta)$  and the other two symmetrically located on the  $\xi$ -axis at a distance c from the origin. Note that the positions of corresponding peaks in both terms coincide and that the lateral peak height is proportional to  $|\mu|$ .
- The third term in Eq. (10) provides the information about the modulation of the Young interferograms by Michelson fringes. This term describes two sets of peaks with pyramidal profiles, given by the convolution of the *rect* functions. These sets are located symmetrically with respect to the origin of coordinates at (X,Y) and (-X,-Y) respectively, and their peaks are distributed according to  $H(\xi)$ .

Each set has a principal peak, given by the first delta function of  $H(\xi)$ . Its height provides only information about |v|. The remaining peaks are distributed symmetrically with respect to the principal one, but their heights decay rapidly because they are proportional to products of the form  $|v| |\mu|^m$ , with m an integer (Fig.3).

Therefore, for measuring purposes let us consider the principal peak of one of the sets, say that located at (X,Y). Its mathematical form is given by [Eq. (10)]

$$\frac{I_0}{\pi^2} \frac{|\nu|}{2} \operatorname{rect}\left(\frac{\xi}{a}, \frac{\eta}{b}\right) \otimes \operatorname{rect}\left(\frac{\xi}{a}, \frac{\eta}{b}\right) e^{i\frac{k}{z}(X\xi + Y\eta)} \otimes \delta(\xi, \eta) \otimes \delta(\xi, \eta) e^{i\frac{k}{z}X\xi} \otimes \delta(\xi - X, \eta - Y).$$
(13)

It is apparent that the height of this peak is proportional to |v|.

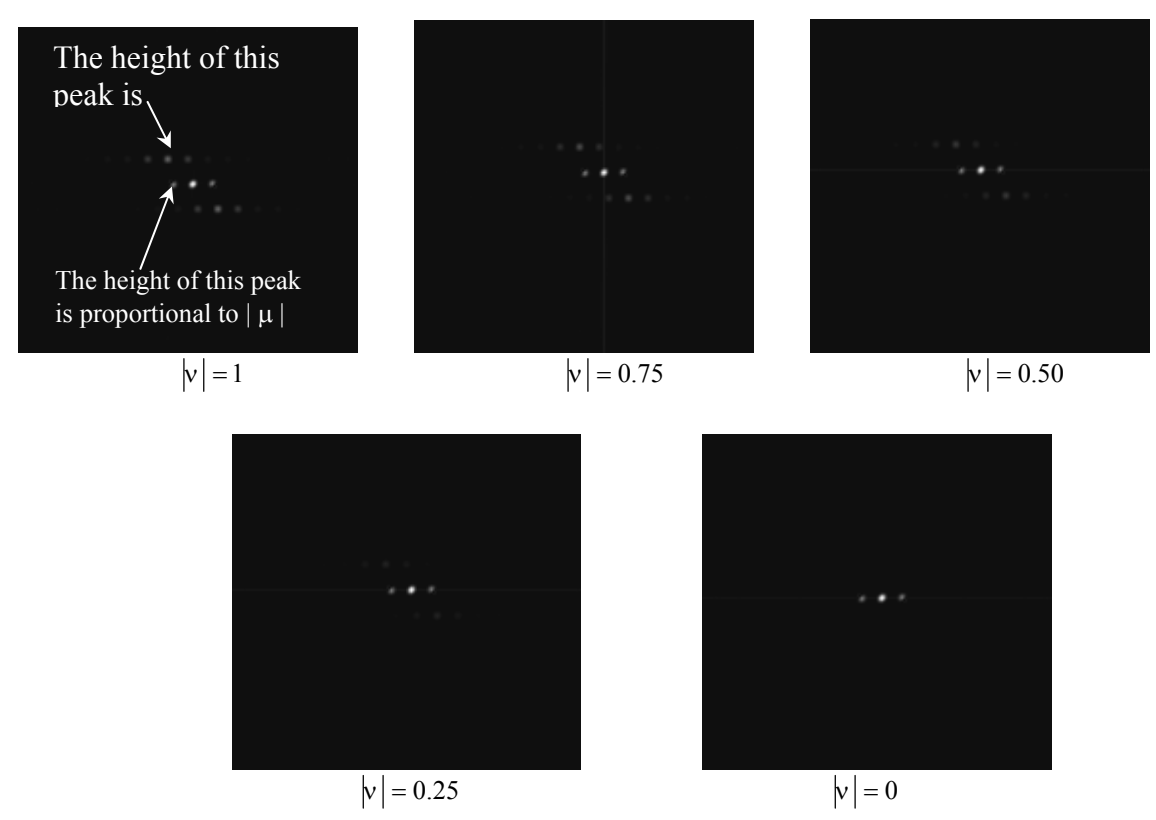
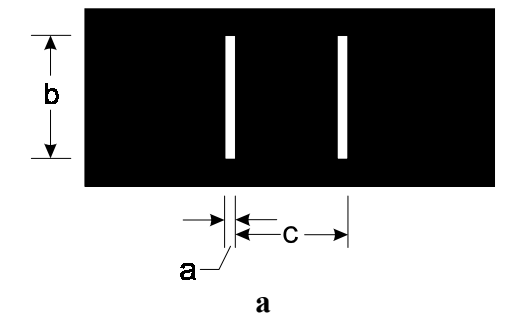


Fig. 3: Fourier spectrum modula of the simulated interferograms in Fig.2

In summary, by looking at only two peaks of  $\tilde{I}(\xi,\eta)$  we can obtain separate measurements of  $|\mu|$  and  $|\nu|$ , as it can see from Fig. 3. For the experiments we have used three Young's slit pairs with the following parameters (Fig. 4a):



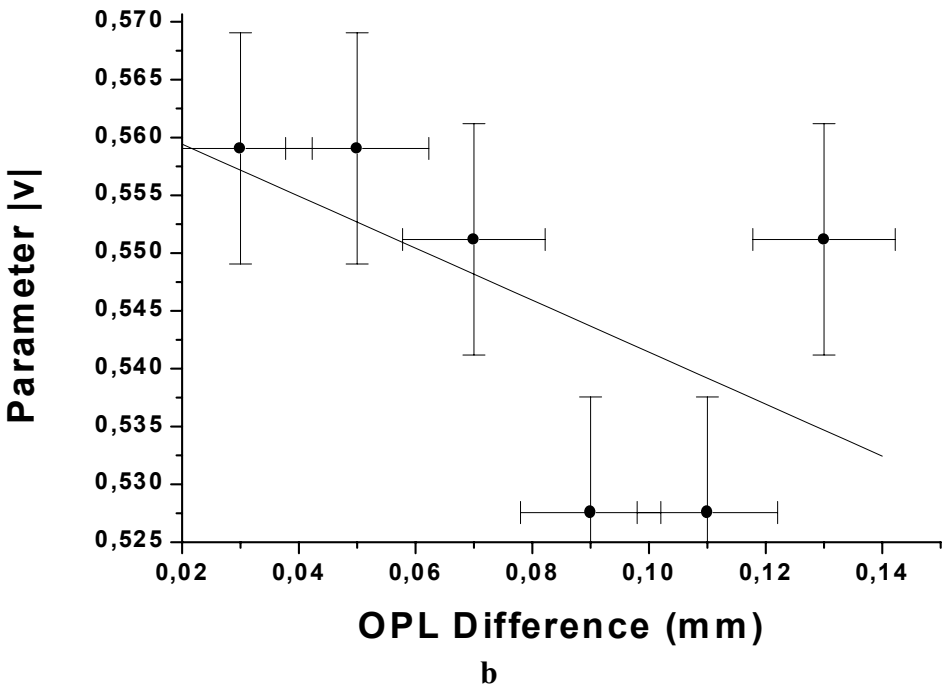


Fig. 4: (a) Geometrical parameters of the Young's slit pairs. (b) Graph of the fringe visibility for the compensated Michelson interferometer alone

- $Y_1$ : a = 0.1 mm., b = 10 mm. c = 0.2 mm.
- $Y_2$ : a = 0.1 mm., b = 10 mm., c = .0.3 mm.
- $Y_3$ : a = 0.1 mm., b = 10 mm., c = 0.4 mm.

A He-Ne laser was used as illumination source. Its coherence length was significantly greater than both the maximum value of the c parameter of the Young's slits and the optical path difference introduced by tilting the mirror of the Michelson's interferometer. This condition was assured by determining the visibility curve of the fringe patterns generated by the compensated Michelson interferometer alone (Fig. 4b). The visibility decay occurs at the level of a percent. Therefore, the effects of temporal coherence can be neglected by using this interferometer.

Figure 5 shows the intensity distribution of an experimental interferogram and the numerically calculated modulus of its Fourier spectrum respectively as an example of the experimental results we have obtained.

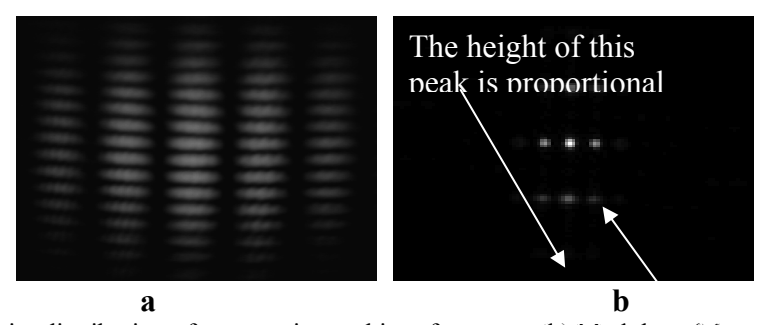


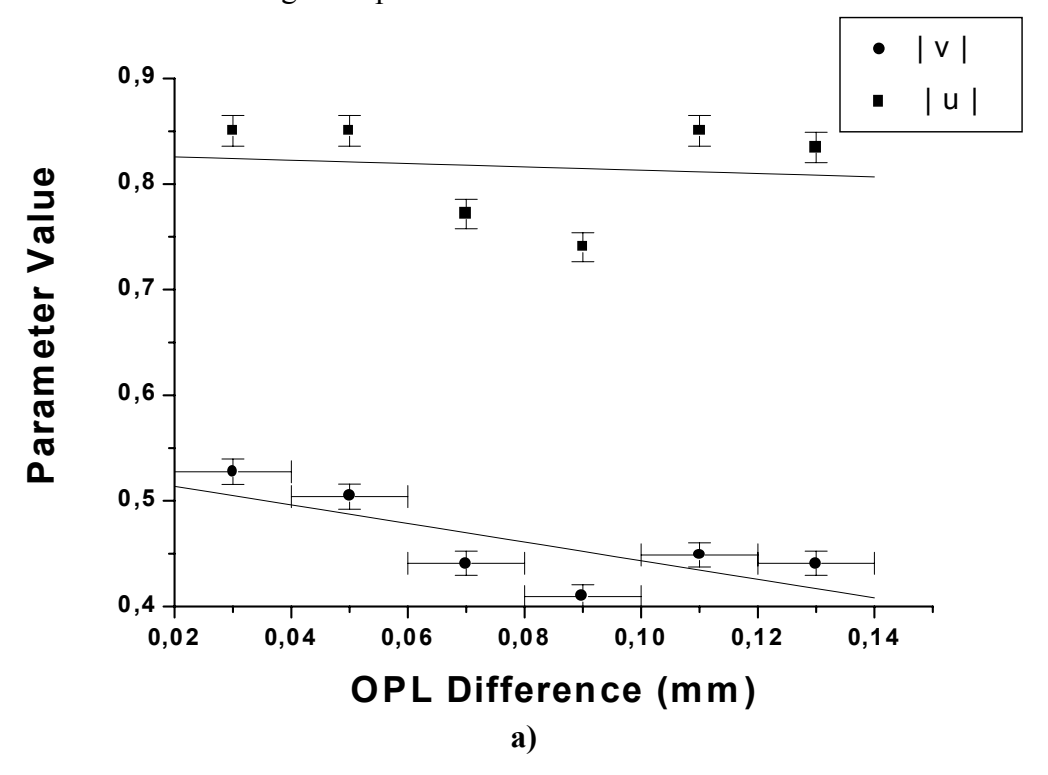
Fig. 5: (a) Intensity distribution of an experimental interferogram. (b) Modulus of the calculated Fourier spectrum of distribution in (a)

Table 1 shows the experimental results for  $|\mu|$  and  $|\nu|$  we have obtained by using the three Young's slit pairs under several optical path length (OPL) differences, corresponding to different tilt angles of the mirror of the Michelson's interferometer [5].

<b>OPL*</b> difference	Young's slit pair Y <sub>1</sub>		Young's slit pair Y <sub>2</sub>		Young's slit pair Y <sub>3</sub>	
[mm]	μ	V	$ \mu $	v	$ \mu $	v
0,03	0,85	0,53	0,89	0,53	0,75	0,44
0,05	0,85	0,50	0,84	0,50	0,75	0,42
0,07	0,77	0,44	0,81	0,45	0,66	0,38
0,09	0,74	0,41	0,88	0,45	0,66	0,36
0,11	0,85	0,45	0,87	0,47	0,73	0,42
0,13	0,83	0,44	0,87	0,39	0,74	0,38

TABLE 1: Experimental results for  $|\mu|$  and  $|\nu|$ 

Figure 6 shows the dependency of the parameters  $|\mu|$  and  $|\nu|$  with respect to the OPL differences for each Young's slit pair. The curves are based on the data in Table 1.



<sup>\*</sup> Optical Path Length. The OPL differences were introduced by different tilt angles of the mirror of the Michelson's interferometer. For all measurements an uncertainty of  $\pm$ 0,01 must be added.

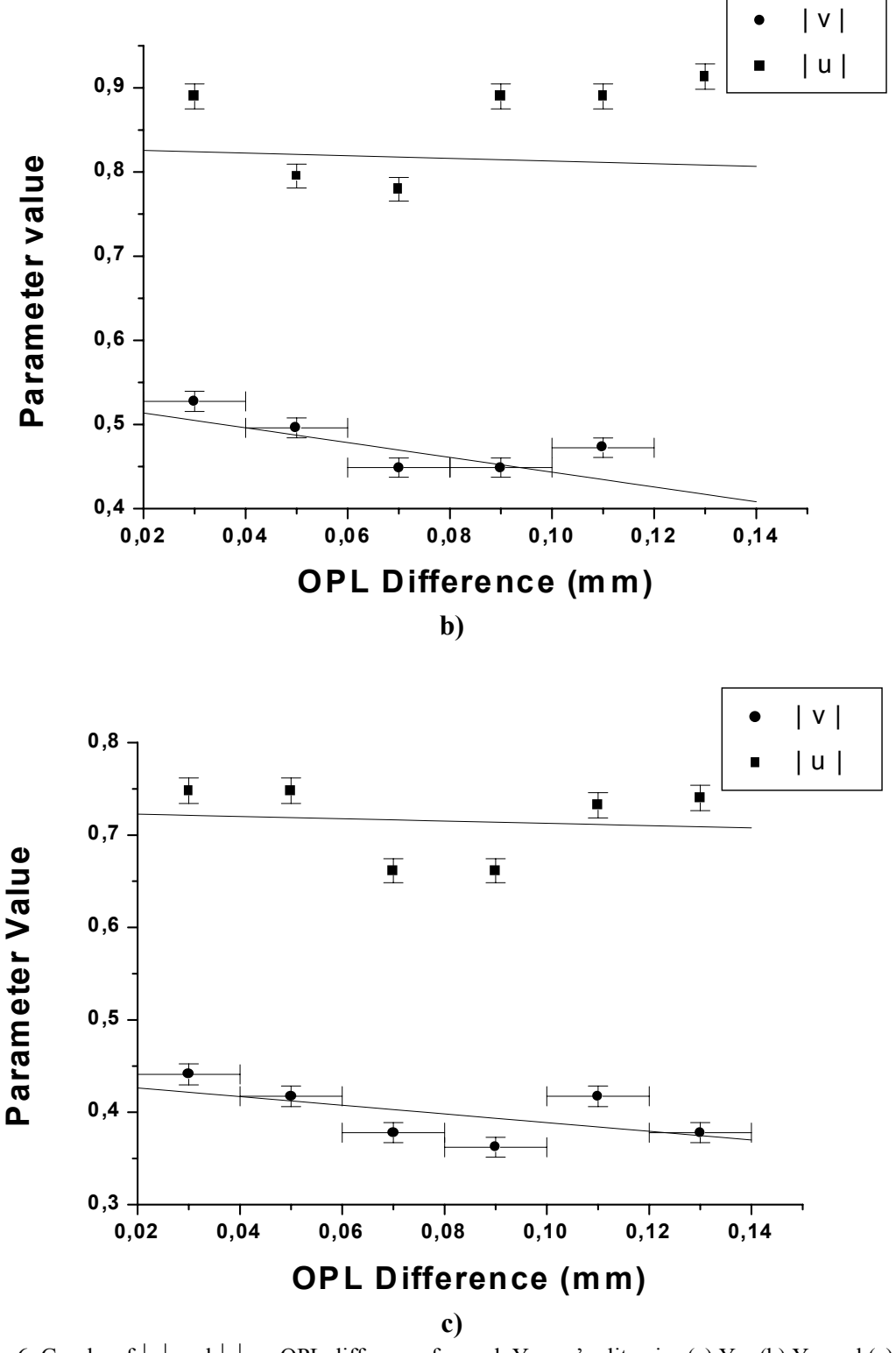


Fig. 6: Graphs of  $|\mu|$  and  $|\nu|$  vs OPL difference for each Young's slit pair: (a)  $Y_1$ , (b)  $Y_2$ , and (c)  $Y_3$ .

As expected,  $|\mu|$  exhibits a high value with small variations in all cases;  $|\nu|$ , however, decays with an appreciable slope as the OPL difference increases, remaining always smaller than  $|\mu|$ . By comparing Fig 4.b with Fig 6 it can be seen that variations on the  $|\nu|$  parameter are one magnitude order faster in the Young-Michelson than in the Michelson interferometer for the same ranging of change of the OPL. It means that, meantime the |v| parameter variations are registered on the hundreds for the OPL changin range from 0.02 to 0,14 mm for the Michelson interferometer, for exactly the same OPL changing range the variations registered on the |v| parameter are on the tenths for the Young-Michelson interferometer. This behaviour persists as the slit pair separation increases, the Young's fringes of the interferograms always exhibiting a high visibility and the loss of visibility in the Michelson's fringes being apparent.

Because of the above results, i.e. theirs independet behaviour for the same condictions, it seems to exist a separability of the parametes  $|\mu|$  and  $|\nu|$ , and the spatial meaning of  $|v(x_1, y_1; x_2, y_2)|$ , we conclude that these parameters denote different properties of the spatial coherence of the source. The primary correlation properties of the optical field, which are established by the module of the complex degree of spatial coherence, remain practically the same in all experimental situations. However, the decay of  $|v(x_1, y_1; x_2, y_2)|$  reveals a finer structure of the spatial coherence, which cause the loss of visibility in the Michelson's fringes of the interferograms.

As a consequence, both  $\mu_0(\xi_1 - \xi_2; \eta_1 - \eta_2)$  and  $v(x_1, y_1; x_2, y_2)$  should be used as descriptors of the spatial coherence properties of light sources revealed by the Young-Michelson interferograms.

This work was performed at the Abdus Salam International Centre for Theoretical Physics (AS-ICTP, Trieste – Italy)). The authors express their acknowledgements to the AS-ICTP for the financial support and to Prof. Franco Gori for his inspiring discussions. Jorge Garcia-Sucerquia thanks the Fundacion Mazda para el Arte y la Cultura and the Fondo para apoyar Trabajos de Grado de Pre- y Posgrado de la Universidad de Antioquia. Francisco F. Medina undertook this work with the support of the ICTP Programme for Training and Research in Italian Laboratories.

## REFERENCES

- 1. Glauber, R. Quantum Theory of Optical Coherence. Phys. Rev. 130 (1963) 2529-
- 2. Mandel, L. and E. Wolf. Optical Coherence and Quantum Optics. Cambridge University Press, Cambridge, 1995.
- 3. Born, M. and E. Wolf. *Principles of Optics*. 2<sup>nd</sup> Ed. Pergamon Press, Oxford, 1964.
- 4. Gaskill, J. Linear Systems, Fourier Transforms and Optics. John Wiley & Sons, New York, 1978
- 5. Garcia-Sucerquia, J. Estructura de la Coherencia Espacial en campos Ópticos Clásicos. Magister Tesis, Universidad de Antioquia, 1999.
- 6. Gradshteyn, I.S., I.M. Ryzhik. Table of integrals, series and products. 5<sup>th</sup> ed., Academic Press, Boston, 1994.

# FIGURE CAPTIONS

- Fig. 1: Experimental set-up of a Young-Michelson interferometer
- Fig. 2: Simulated intensity distributions of interferograms at the exit of a Young-Michelson interferometer
- Fig. 3: Fourier spectrum modula of the simulated interferograms in Fig.2
- Fig. 4: a. Geometrical parameters of the Young's slit pairs
  - b. Graph of the fringe visibility for the compensated Michelson interferometer alone.
- Fig. 5: a) Intensity distribution of an experimental interferogram.
  - b) Fourier spectrum module of a)
- **Fig. 6:** Graphs of  $|\mu|$  and  $|\nu|$  vs OPL difference for each Young's slit pair: a)  $Y_1$ 
  - b) Y<sub>2</sub> and c) Y<sub>3</sub>